N^6-Methyladenosine methylome landscape and a novel m^6A-related gene risk signature associated with the prognosis of glioblastoma

Rongrong Zhao
Shandong University Qilu Hospital
Boyan Li
Shandong University Qilu Hospital
Zheng He
Shandong University Qilu Hospital
Shouji Zhang
Shandong University Qilu Hospital
Qindong Guo
Shandong University Qilu Hospital
Ping Zhang
Shandong University Qilu Hospital
Wei Qiu
Shandong University Qilu Hospital
Yanhua Qi
Shandong University Qilu Hospital
Shulin Zhao
Shandong University Qilu Hospital
Ziwen Pan
Shandong University Qilu Hospital
Xing Guo
Shandong University Qilu Hospital
Hao Xue (xuehao@sdu.edu.cn)
Shandong University Qilu Hospital
Gang Li (dr.ligang@sdu.edu.cn)
Shandong University Qilu Hospital

Research Article

Keywords: N6-methyladenosine, glioblastoma, m6A-related gene risk signature, prognosis, clinical prediction model

Posted Date: March 19th, 2021

DOI: https://doi.org/10.21203/rs.3.rs-300744/v1

Abstract

Background

N^6-Methyladenosine (m^6A) represents one of the most prevalent mRNA modification, strongly linked to the initiation and progression of glioblastoma (GBM). However, the global transcriptome-wide patterns of m^6A in GBM are largely unknown.

Methods

RNA m^6A modification patterns in GBM and normal brain tissues were described via m^6A-sequencing (m^6A-seq). Least absolute shrinkage and selection operator (LASSO) regression and multivariate Cox regression analyses were performed to identify genes for constructing an m^6A-related gene risk signature. A nomogram was developed by integrating the risk signature with clinicopathological factors. Time-dependent receiver operating characteristic (ROC) curves were used to evaluate the performance of the prognostic model.

Results

Here, we reported transcriptome-wide m^6A modification profiling in GBM and normal brain tissues for the first time, illuminating highly differences between these two groups, showing that m^6A regulates large number of genes and cancer-related pathways. We demonstrated an m^6A-regulated 8-gene risk signature that correlated with poor prognosis of GBM patients from the TCGA dataset, and validated its efficiencies in LeeY, Gravendeel and CGGA datasets. Furthermore, we developed a nomogram that integrated the risk signature with clinicopathological factors and validated its better performance for predicting the 1-, 3- and 5-year survival rates of GBM patients.

Conclusion

This study presents the first m^6A transcriptome-wide map of human GBM and normal brain tissues, whose m^6A landscape is greatly altered in GBM; In addition, an epigenetic m^6A-related 8-gene risk signature and a nomogram are established, whose efficiencies have a high potential to further improve the individualised therapy in GBM patients.

Background

N^6-Methyladenosine (m^6A) is the most prevalent methylation modification of mRNAs in eukaryotes[1, 2], and it regulates almost every aspect of mRNA metabolism, including mRNA splicing[3], translation[4, 5], stability[6] and decay[7], regulating gene expression at the posttranscriptional level. RNA m^6A modification

is catalysed by the m^{6}A methyltransferase complex (MTC), which is composed of methyltransferase-like 3 and 14 (METTL3 and METTL14, respectively) and their cofactors, Wilms tumour 1-associated protein (WTAP), KIAA1429 and RBM15. m^{6}A is removed by m^{6}A demethylases, such as FTO and ALKBH5, and detected by 'm^{6}A readers', including YTHDF1/2/3, YTHDC1/2, IGF2BP1/2/3 and others, which interact with distinct subsets of m^{6}A sites to mediate different effects on mRNA metabolism, keeping m^{6}A modification in a dynamic balance[8]. An increasing number of validation studies show that dysregulation of the m^{6}A modification and its associated enzymes also lead to the initiation and progression of tumours[9]. With the progress of high-throughput technologies, two independent studies reported the m^{6}A RNA methylomes in mammalian genomes for the first time by the m^{6}A-RNA immunoprecipitation approach followed by high-throughput m^{6}A-sequencing (m^{6}A-seq) in 2012[1, 10]. These studies provided a method to elucidate the m^{6}A modification pattern on a transcriptome-wide level and help to get further insight into the positions and roles of m^{6}A in mRNA metabolism. However, the global transcriptome-wide patterns of m^{6}A in most kinds of cancers, including glioblastoma (GBM), are largely unknown.

GBM is an intractable central nervous system tumour without effective therapy strategies. While the study of m^{6}A in GBM is in its early stages, studies in this field have drawn controversial conclusions. Researches collected so far clearly demonstrate that the levels of mRNA m^{6}A levels impacts multiple aspects of GBM[11–15], including proliferation, glioma stem cell (GSC) self-renewal and tumorigenesis, prompting us that the mRNA m^{6}A modification may be a promising target for GBM therapy. However, there is no comprehensive study on the expression of m6A RNA methylation patterns in GBM tissues.

Here, we report transcriptome-wide m^{6}A profiling in GBM and normal brain tissues via m^{6}A-seq for the first time, illuminating the highly diverse m^{6}A modification differences between these two groups. Through a systematic analysis, we found that abnormal m^{6}A RNA modifications in GBM regulate the expression of a large number of genes and cancer-related pathways. We demonstrated an m^{6}A-regulated 8-gene risk signature with poor prognosis of GBM patients from the Cancer Genome Atlas (TCGA) dataset and validated the 8-gene risk signature in the LeeY, Gravendeel and Chinese Glioma Genome Atlas (CGGA) datasets. Furthermore, we developed a nomogram that integrated the m^{6}A-related 8-gene risk signature with clinicopathological factors and validated its superior performance in predicting prognosis of GBM patients. We hope this study will facilitate further investigations of the potential roles of the m^{6}A modification in GBM pathogenesis.

Results

Overview of N^6-methyladenosine methylation within mRNAs in GBM and normal brain tissues

To understand the role of the m^{6}A modification in GBM, three human GBM tumour tissues versus three normal brain tissues from patients were selected for transcriptome m6A-sEq. A total of 15804 m^{6}A peaks were identified by model-based analysis of MACS2 software in the tumour group, representing transcripts of 9228 genes (Table 1); in the normal group, 12356 m^{6}A peaks were identified, which corresponded with the transcripts of 8320 genes (Table 2). The protein-coding RNAs (mRNAs) constituted the majority of the m^{6}A-modified RNAs (over 75% of all m^{6}A-modified genes in the normal and GBM groups); other RNA types were also present, such as lncRNAs, pseudogenes and others (Fig. 1A). The validity and stringency of our m^{6}A-seq data were confirmed by an unbiased search for motifs enriched m^{6}A peak region, and the previously reported top m^{6}A consensus motif 'GGAC' was identified in both tissue groups (Fig. 1B), similar to previous studies[16, 17]. Further, we found that 68.6% of the m^{6}A-methylated genes in the normal group (57.1% of the methylated genes in the GBM group) contained only one peak, while a relatively small number of genes contained two or more peaks (Fig. 1C), consistent with the proportion trend previously reported in mouse brains[2]. Current studies have found that the degree and pattern of methylation of mRNAs can affect their splicing, translation, decay and other RNA metabolism, regulating protein expression post-transcriptionally. To this end, we started systematically examining the distribution landmarks of m^{6}A peaks along mRNAs. We found that there are m^{6}A peaks throughout the genes but with a obvious enrichment around the stop codons, also extended to the 3' UTR region (Fig. 1D). To further analyse the distribution profiles of m^{6}A peaks within mRNAs, peaks were categorized into five transcript segments—the 5' UTR, TSS (100 nucleotides centred on the start codon), coding sequence (CDS), stop codon segment (100 nucleotides centred on the stop codon) and 3' UTR (Fig. 1E, pie chart)—and then normalized by the relative fraction each segment covered in the transcriptome (Fig. 1E, histogram). Our results showed that the m^{6}A site most often occurred in the 3' UTR, with some near the stop codons, consistent with previous studies that reported mRNA m^{6}A-seq data[1, 2]; the stop codon segment stood out as most enriched peak of the m^{6}A peaks. From these results, we concluded that the m^{6}A modification was particularly harboured around the stop codon, extending into the 3' UTR region in GBM tissues.

Functional analysis of specific genes associated with m ^{6} A peaks in normal brain tissue and GBM tissue

RNA m^{6}A-seq analysis of RNA derived from brain tissues revealed that, in the normal group, there were 9903 overlapping m^{6}A peaks within 7565 mRNA transcripts, representing transcripts of 6565 genes. In the GBM group, there were 13033 overlapping m^{6}A peaks within 9209 mRNA transcripts, corresponding to 7525 genes. The differences and overlaps in m^{6}A genes between the individuals are shown by the Venn diagram in Fig. S1A. Among them, 4257 m^{6}A-modified genes were detected within both groups. Compared with the normal group, the tumour group had 3268 new genes that appeared with the disappearance of 2308 genes, indicating a significant difference in global m^{6}A modification patterns

between the tumour and normal groups. The Metascape database analysis[18] revealed that specific genes with m^{6}A in the normal group were significantly linked to the transmission of neural signals, such as the regulation of ion transport, synaptic signalling, signal release and potassium channels, as well as system development, such as neuronal system, regulation of system process, embryonic morphogenesis and brain development, and these genes interacted with each other significantly (Fig. S1B). The analysis of tumour-specific genes indicated that they were significantly enriched in the metabolism of RNA and ribonucleoprotein complex biogenesis, playing key roles in regulation of the protein expression levels, as well as some terms related to cell growth, such as cell cycle, DNA repair and others (Fig. S1C).

RNA m^{6}A methylation changes between GBM and normal brain tissues

To uncover the biological implications of m^{6}A methylation in GBM, the global abundance of the m^{6}A peaks between GBM and normal brain tissues were compared. In total, 9315 differentially methylated peaks were selected to study further. A total of 3130 hypermethylated m^{6}A sites, corresponding to 2349 protein-coding genes, were found in the GBM group compared with the normal group, and 6185 hypomethylated m^{6}A sites, representing 4472 genes, were discovered (Fig. 2A, fold change $\geq$ 1.2, P $\leq$ 0.05). Consistent with the global distribution of m^{6}A sites in GBM and normal brain tissues, the differentially methylated m^{6}A sites were also preferentially distributed in the CDS and 3' UTR, while the hypomethylated m^{6}A sites preferentially occurred in the 5' UTR, compared with normal brain tissues (Fig. 2B). The genes containing significantly hypermethylated m^{6}A peaks were analysed by the Metascape database, and they were significantly enriched in the cell cycle, cell division, DNA replication, DNA repair, mitotic sister chromatid segregation, RNA splicing, and system development, with the corresponding signalling pathways interacting with each other to form a protein–protein interaction network (Fig. 2C). In addition, the Kyoto Encyclopedia of Genes and Genomes (KEGG) pathway analysis revealed that hypermethylated m^{6}A sites represented genes in the GBM group that were significantly enriched in many pathways involved in cancer pathogenesis, including miRNAs in cancer, cell cycle, and the Hippo, p53, Wnt, TGF-β and Notch signalling pathways (Fig. S2A). Further, genes containing significantly downregulated m^{6}A peaks were analysed by performing Gene Ontology (GO) and KEGG pathway analyses. Similar to the normal-unique m^{6}A-modified genes, these genes were also mainly involved in the transmission of signals and neuronal system development (Fig. S2B-C). These results revealed that abnormally m^{6}A-modified genes, especially hypermethylated m^{6}A genes, were enriched in cancer-related signalling pathways in GBM tissues.

Conjoint analysis of m^{6}A-seq and RNA-seq data of GBM and normal brain tissue samples

TCGA RNA-seq data were used to detect the differentially expressed genes between 154 primary GBM and normal brain tissues. Compared with normal samples, 6397 genes were differentially expressed in primary GBM tissues (fold change $\geq$ 2 and padj $\leq$ 0.05), including 3794 downregulated genes and 2605

upregulated genes (Fig. S3A; Table 3). The differentially expressed genes were selected for Metascape analysis. Similar to the m^{6}A-modified differentially expressed gene enrichment terms, abnormal upregulated genes in GBM samples were significantly enriched in biological processes involving the cell cycle, cell division and some other proliferation-related terms (Fig. S3B), with downregulated genes enriched in the transmission of signal and neuronal system development (Fig. S3C).

By conjoint analysis of m^{6}A-seq and TCGA RNA-seq data, we discovered a positive correlation of differentially methylated m^{6}A peaks and gene expression levels in GBM and normal tissues. All genes were mainly divided into four groups, including 957 hypermethylated as well as upregulated genes ('hyper-up'), 1975 hypomethylated as well as downregulated genes ('hypo-down'), 312 hypermethylated but downregulated genes ('hyper-down') and 173 hypomethylated but upregulated genes ('hypo-up'). The number of hyper-up and hypo-down genes were greater than the number of hyper-down and hypo-up genes (Fig. 2D), indicating that m^{6}A modification level of these genes tend to have a positive correlation with their corresponding mRNA expression in GBM. Furthermore, a large cohort of transcripts contained m^{6}A peaks that were not regulated at the mRNA level, emphasizing that other RNA metabolic processing steps of these genes, such as transport or translation, may be fine tuned by m^{6}A. Since hyper-up and hypo-down genes covered the vast majority of the number of differentially regulated genes, both in m^{6}A modification and expression levels, we focused on these genes in the following work. The two parts of the RNA transcripts were divided into subgroups according to their m^{6}A modification sites. We found that the m^{6}A sites of the regulated genes were also mostly in the 3' UTR, followed by CDS, in accordance with the global m^{6}A distribution. We found no significant correlations between the location of m^{6}A sites and their corresponding transcript expression level (Fig. 2E), emphasizing the complexity of m^{6}A functionality. Further, Metascape database analysis revealed that these hyper-up genes were mainly enriched in the regulation of cell biological functions, including cell division, cell cycle phase transition, extracellular structure organization, cell cycle checkpoints, chromosome segregation, regulation of cell adhesion and others. Additionally, these genes and enriched terms were of great importance to the protein–protein interaction network clusters (Fig. 2F). KEGG pathway analysis similarly showed that these terms were linked to cell proliferation regulation pathways, such as the cell cycle and DNA replication, as well as classical signalling pathways involved in cancer development, including p53 signalling pathways, PI3K-Akt signalling pathways and microRNAs in cancer and others (Fig. S4A). Similar to the function of the normal-specific genes, the hypo-down genes were also mainly enriched in the transmission of neural signals and system development, and the results of the enriched terms and network of enriched terms are shown in Fig. S4B. These results suggested that the hyper-up m^{6}A genes were closely involved in cancer-related signalling pathways in GBM tissues.

Weighted gene co-expression network analysis (WGCNA) and key module identification

To determine the phenotypic relevance of the hyper-up genes, we identified gene modules (groups of highly interconnected genes), highly associated with clinicopathological features of GBM via WGCNA

method [19]. A hierarchical clustering tree, in which each leaf on the tree represented a single gene and genes with similar expression data were close linked and formed a branch of the tree, on behalf of a gene module, was constructed using dynamic hybrid cutting and merged dynamic cutting. Five modules were generated (Fig. 3A-B). We were interested specifically in the oncogenes inducing GBM tumorigenesis, and among the five modules, the turquoise module was the most highly correlated with GBM tumorigenesis (r = 0.34, p = 2e-05), and the brown module was moderately correlated with carcinogenesis (r = 0.3, p = 1e-4). The correlation between the other modules and GBM was less than 0.3 (Fig. 3C). Furthermore, only genes in the turquoise module had a greater significance with the corresponding module (Fig. 3D, correlation r = 0.43, p = 9.2e-13) and were considered to be more connected with disease progression, and the other modules did not have a significant correlation with their corresponding genes (Fig. S5). Thus, the turquoise module was identified as a hub module to explore in the following work. The highly correlated genes in the turquoise module were investigated as potential key genes associated with GBM tumours. Based on the cut-off standard (module membership > 0.8), a total of 58 genes that were highly correlated to the turquoise module were defined as candidate hub genes (Fig. 3D). Next, 44 genes included in both the turquoise module and TCGA HG-UG133A platform dataset were analysed through the GO database. GO biological process analysis showed that almost all of them could be involved in cell cycle processing, and some of them played a key role in cell division and nuclear division. GO cellular component analysis showed that the cell cycle-regulating genes were mostly in the nucleus, with some of them located in chromatin. GO molecular function analysis revealed that some of the proteins coded by these genes can bind to ATP and enzymes, suggesting that they could participate in cell signal transduction and metabolism. We visualized the genes enriched in GO database annotation terms via circos string graphics, ranked by logFC in descending order (Fig. S6). These results indicated that the 44 genes played an important role in regulating GBM progression.

LASSO Cox regression identifying an m^{6}A-related 8-gene risk signature

The 44 genes from the above analysis were used to construct a gene expression profile with a total of 522 primary GBM patients in the TCGA HG-UG133A platform, and LASSO regression analysis was performed on these genes to prevent overfitting problems in the risk signature. A total of 8 m^{6}A-related genes—aurora kinase B (AURKB), cell division cycle 25C (CDC25C), centromere protein E (CENPE), epithelial cell transforming 2 (ECT2), forkhead box M1 (FOXM1), kinesin family member C1 (KIFC1), minichromosome maintenance complex component 10 (MCM10) and thyroid hormone receptor interactor 13 (TRIP13)—were identified according to the optimal lambda value (Fig. 3E-F). As described in the methods section, the risk signature was established based on their expression levels, and the regression coefficient parameter were calculated via the multivariate Cox regression model (formula in additional file 2 in the Supplementary methods section) was used to predict the risk score of patients, dividing genes into a high-risk group (n = 261) and a low-risk group (n = 261) according to the median cut-off value of the scores (Fig. 4A). The survival status is shown in Fig. 4B in ascending risk score order. The Kaplan–Meier curve analysis showed that the overall survival of patients in the low-risk group is

significantly better than those in the high-risk group in quartile cut-off values (Fig. 4C, HR: 2.129 [1.597–2.839], P□0.0001). Further, ROC curves were performed to compare the efficiencies of the prognostic risk model. ROC curves showed that the areas under the curve (AUCs) of the risk signature for predicting the 1-, 3- and 5-year survival rates were 0.628, 0.763 and 0.844 (Fig. 4D), respectively.

To study the relationship between the risk signature and clinical factors, we compared the risk scores stratified by molecular subtypes, IDH1 status, MGMT promoter status and G-CIMP status in the TCGA GBM cohorts, separately. As shown in Fig. S7A, the risk scores were lower in patients with a mutation in IDH1 than in those with wild-type IDH1. The risk scores of samples with MGMT promoter methylation were lower than those of patients with an unmethylated MGMT promoter. For G-CIMP status, the risk scores were lower in patients with G-CIMP than in those without G-CIMP. The risk scores in the proneural subtype were obviously lower than those in the classical and mesenchymal subtypes. Older patients (> 55 years) had higher risk scores than younger patients (≤ 55 years). However, there were no differences in risk scores between males and females. Subsequently, we also evaluated the prognostic efficiency of the risk signature in different cohorts stratified by the MGMT promoter status, IDH1 status, G-CIMP status and molecular subtypes. As shown in Fig. S7B, Kaplan–Meier curve analysis showed that patients in high-risk groups with these clinical characteristics had more adverse outcomes than those in the low-risk group without these clinical characteristics according to the median or quartile group cut-off value.

AURKB, CDC25C, CENPE, ECT2, FOXM1, KIFC1, MCM10 and TRIP13 were the 8 m^6A-related genes in our LASSO Cox model. Then, we analysed the protein interaction relationship via the STRING database and found that they can interact with each other. Further, GO analysis showed that all of these genes could be involved in mitotic cell cycle processing, and KIFC1, AURKB, CENPE, CDC25C and ECT2 played a key role in cell division. GO cellular component analysis showed that all of them located in the nucleus, with KIFC1, AURKB, CENPE, CDC25C, FOXM1 and ECT2 located in the spindle. GO molecular function analysis showed that some of them could bind with a kinase or ATP (Fig. 4E). The Gene Expression Profiling Interactive Analysis (GEPIA) database analysis showed that all 8 genes had a higher expression level in GBM tumour tissues than in normal tissues in the GETx dataset (Fig. 4F). The m^6A characteristics of the 8 genes are shown in Table S1, with some of them having two or more modification sites, and the gene plot of the methylation information of these genes is shown in Fig. S8. And the core component of the m^6A methylase complex, METTL3, has a significant positive correlation with these 8 genes in TCGA GBM cohort (Fig. 4G). MeRIP qPCR data also showed that the 8 genes were highly m^6A modified (Fig. 4H). Further, compared to the NC group, the expression level of these 8 genes decreased significantly after knocking down METTL3(Fig. 4I). These results indicated that the 8 genes showed high efficiency in distinguishing tumours from normal tissues in terms of gene expression level and m^6A methylation level, predicting unfavourable prognosis in GBM patients.

Validating the efficiencies of the 8-gene m^6A-related epigenetic signature in the three datasets

To validate the efficiencies of the 8-gene m^6A-related epigenetic signature, we collected a total of 191 GBM samples from the LeeY microarray dataset, 155 GBM samples from the Gravendeel microarray dataset and 133 GBM samples from the CGGA RNA-seq dataset as three validation datasets to evaluate the efficiency of the risk signature; the clinicopathological characteristics of the validation patient cohorts are shown in Table S2. Using the same methods as for the TCGA discovery cohort, the risk scores of patients were calculated on the basis of the expression levels of the eight genes in the three validation cohorts and were then divided into a high-risk group and a low-risk group based on the median cut-off value of the risk scores (Fig. 5A), with the survival status in an ascending order of risk score shown in Fig. 5B. In agreement with the initial discovery of the TCGA cohort findings, the Kaplan–Meier survival curves showed that patients in high-risk group had poorer prognosis than those in low-risk group (Fig. 5C, LeeY dataset, HR: 1.737 [1.281–2.354], P = 0.0001; Gravendeel dataset, HR: 2.008 [1.43–2.82], P < 0.0001; CGGA dataset, HR: 1.906 [1.301–2.793], P = 0.005). The AUCs of the 1-, 3- and 5-year for predicting survival rates of GBM in the LeeY dataset were 0.59, 0.692 and 0.86, respectively; those in the Gravendeel dataset were 0.674, 0.885 and 0.863, respectively; and those in CGGA dataset were 0.517, 0.744 and 0.658, respectively (Fig. 5D). The expression levels of these 8 genes in 4 different datasets of GBM are shown in Fig. S9A-B. All 8 genes showed relatively upregulated expression in the high-risk group compared with that in the low-risk group. The high-risk group had more elderly patients and classical and mesenchymal subtype patients, whereas samples with G-CIMP status were almost all in the low-risk group in the LeeY and Gravendeel datasets, with complete clinical information (Fig. S9B). Concomitantly, the Kaplan–Meier curve analysis results indicated that all 8 genes could be independent adverse prognostic factors in the CGGA and LeeY datasets (Fig. S10). These results demonstrated the robustness of our m^6A-related 8-gene risk signature in predicting unfavourable prognosis in GBM patients.

Functional enrichment analysis of the risk signature

To explore the functional enrichment pathways related to the risk signature, 532 TCGA GBM patients were divided into the high-risk group (top quartile, n = 130) and low-risk group (bottom quartile, n = 130) on the basis of the quartile risk score. Then differential expression analysis was conducted, and compared with the genes in the low-risk group, a total of 4357 genes were differentially regulated in the high-risk group, out of which 4205 genes were upregulated and only 152 genes were downregulated (Fig. S11A-B, fold change ≥ 1.2 and Padj ≤ 0.05, Table 4). The MSigDb hallmark pathway analysis of the upregulated genes showed that signs of cancer-related hallmarks, e.g., epithelial–mesenchymal transition, glycolysis, mTOR signalling, apoptosis, E2F targets, G2M checkpoints and others, were significantly enriched (Fig. S11C); the detailed information is shown in Table 5. To further understand the function of these high-risk-related upregulated genes, KEGG pathway enrichment analysis was performed. As shown in Fig. S11D, cancer-related pathways, such as DNA replication, apoptosis, and cell cycle pathways, could be enriched significantly; the detailed information of all enriched clusters is shown in Table 6. Furthermore, Gene Set Enrichment Analysis (GSEA) suggested that the malignant hallmarks of tumours, including the apoptotic signalling pathway, cell cycle and pathway in cancer, were significantly associated with the high-risk score group (Fig. S11E). All these results suggested that the risk signature was closely related to the malignancy of GBM.

Construction of a nomogram for predicting the 1-, 3- and 5-year survival rates of GBM

To better apply the m^{6}A-related 8-gene risk signature, we collected 334 GBM patients in the TCGA HG-UG133A platform with detailed clinicopathological parameters, including IDH1 status, G-CIMP status, age and therapy history (Table S3). Then, we randomly divided the 334 samples into a training cohort and a validation cohort. The training cohort was used to construct a nomogram to predict the survival rate of GBM patients, and the validation cohort was used to further evaluate the effectiveness of the nomogram. First, we performed univariate and multivariate Cox regression analyses in the training cohort, both of which indicated that the risk signature was an independent risk factor for patients with GBM (Fig. 6A, $P < 0.001$). IDH1 mutant status was a significant protective factor for GBM in the univariate analyses, while the multivariate analyses showed that IDH1 status was not a significant factor. Subsequently, a nomogram integrating the five factors, without the IDH1 status factor, was constructed for predicting the 1-, 3- and 5-year survival rates of GBM patients. In the nomogram, the 1-, 3- and 5-year survival rates were estimated by combining the total points for each factor (Fig. 6B). Furthermore, this new combination signature also demonstrated that the m^{6}A-related 8-gene risk signature was a significantly important diagnostic indicator compared to other classic clinicopathological features, including age, sex, G-CIMP status, and treatment. ROC curves were then used to evaluate the reliability of the nomogram. The AUCs for predicting the 1-, 3- and 5-year survival rates were 0.707, 0.904 and 0.966, respectively, in the training cohort and 0.742, 0.839 and 0.918, respectively, in the validation cohort (Fig. 6C). These results indicated that the nomogram demonstrated good accuracy in predicting survival rates in patients with GBM.

Discussion

GBM is an intractable central nervous system tumour without effective therapy strategies. As the most abundant internal modification in eukaryotic mRNAs, the m^{6}A modification was reported to play key roles in various RNA metabolism pathways involved in the initiation and progression of cancers[9]. Nevertheless, to date, the transcriptome-wide distributions of the m^{6}A modification in GBM tumour tissues and normal brain tissues, as well as the specific role of abnormal m^{6}A modifications in GBM pathogenesis, are largely unclear. In this study, we developed a global m^{6}A transcriptome roadmap of GBM tissues versus normal brain tissues for the first time, illustrating that the gene expression levels and cancer-related pathways were modulated by abnormal m^{6}A RNA modifications, and constructed a predictive m^{6}A-related 8-gene risk signature that can better stratify and predict clinical outcomes of GBM patients. The nomogram further improves the predictive power and accuracy of the model.

We analysed the m^{6}A-seq data and determined that the m^{6}A modification pattern in GBM samples was distinct from that of normal brain controls, with 3268 new genes in the tumour group and 2308 genes that disappeared, indicating significant variability in global m^{6}A modifications between the tumour and normal groups (Fig. S1). Analysing the differentially methylated genes revealed that cancer-related

biological processes and pathways were significantly enriched, indicating the relationship between abnormal m^{6}A modifications and GBM pathogenesis. Furthermore, the combined analysis of our m^{6}A-seq and TCGA mRNA-seq data revealed 957 genes in the GBM group, which had hypermethylated m^{6}A peaks along with significant upregulation changes in mRNA abundance compared with the normal brain group (Fig. 2D). These genes play a crucial role in the progression of GBM and are worth further investigation. Then, WGCNA, LASSO regression and multivariate Cox regression analyses were used to identify genes to construct a risk signature; a total of 8 m^{6}A-related genes (AURKB, CDC25C, CENPE, ECT2, FOXM1, KIFC1, MCM10 and TRIP13), which were associated with GBM survival, were identified. A large number of studies suggest that AURKB[20], CDC25C[21, 22], CENPE[23], ECT2[24], FOXM1[25–27], KIFC1[28], MCM10[29, 30], and TRIP13[31, 32] are overexpressed during cancer progression, can promote cell proliferation, and contribute to tumour formation, including the formation of GBM, consistent with our findings that these genes can be independent risk factors for GBM survival (Fig. S10). Notably, the m^{6}A demethylase ALKBH5 can demethylate FOXM1 nascent transcripts, leading to enhanced FOXM1 expression and to the malignant development of GBM[27]. ECT2, which belongs to the YTHDF class of YTH proteins and is characterized by several groups, can serve as an m^{6}A reader to regulate RNA metabolism in plants[10, 33]; therefore, further exploration of these genes is worthy of future research. Additionally, some of these genes exhibit a certain mutual regulation relationship[34, 35], reaffirming the database analysis results (Fig. 4E). Further functional studies may help to clarify the molecular mechanisms of the abovementioned genes in the development of GBM. Moreover, the expression of these genes can be positively regulated by the m^{6}A modification in high-throughput sequencing data, and our gene-specific m^{6}A qPCR assays also confirmed that all 8 genes can be highly modified by m^{6}A. So far, enzymes or factors that catalyse, recognize, and remove m^{6}A have been identified, illustrating the functional importance of the underlying molecular mechanisms of the m^{6}A modification machinery. Although, we showed that METTL3 could regulate the expression in a positive manner both in the database and our experiments (Fig. 4G-I), it also requires further verification in the future to clarify the specific regulation mechanism. These findings can aid in the search for therapeutic interventions against the dysregulated m^{6}A machinery to treat cancers. In the present study, we only analysed the genes with mRNA expression level changes. It was previously reported that the m^{6}A modification could also influence the localization, transportation and translation of target mRNAs that depend on the recognition of different kinds of ‘readers’[36]. Therefore, functional and mechanistic experiments are needed to further confirm the regulatory roles of m^{6}A RNA modifications on the other genes without expression changes in GBM, which may also provide theoretical guidance for the future treatment of GBM.

Conclusion

In conclusion, this study presents the first m^{6}A transcriptome-wide map of human GBM and normal brain tissues, whose m^{6}A landscape is greatly altered in GBM, and an epigenetic 8 m^{6}A-related gene signature and a nomogram are established, which can be used as independent prognostic markers and accurate

clinicopathological parameter predictors. The comprehensive evaluation of individual GBM m^6A modification pattern will contribute to enhancing our understanding of the tumor initiation and malignant progression, prompting us that modulation of epi-transcriptomic processes such as m^6A methylation might be an interesting target for GBM therapeutic interventions.

Materials And Methods

Patients and specimens

Human GBM tissues and normal brain tissues (the cortex of decompressive surgery patients with brain trauma or hypertensive intracerebral haemorrhage) were obtained from patients admitted to Qilu Hospital from November 2017 to December 2019. All participants provided written informed consent, and the research was approved by the Ethical Committee on Scientific Research of Shandong University Qilu Hospital (approval number: KYLL-2018-324).

Data acquisition

The TCGA GBM RNA-seq transcriptome data and corresponding clinicopathological information of GBM patients were obtained from the TCGA database (http://cancergenome.nih.gov/). The TCGA HG-UG133A platform microarray data were obtained from https://xena.ucsc.edu/public, and corresponding clinicopathological parameters of GBM patients were obtained from the Gliovis database (http://gliovis.bioinfo.cnio.es/). The CGGA GBM RNA-seq transcriptome data and corresponding clinicopathological parameters of GBM patients were obtained from the CGGA database (http://www.cgga.org.cn/). The LeeY dataset and Gravendeel dataset microarray data and corresponding clinicopathological parameters of GBM patients were obtained from the Gliovis database (http://gliovis.bioinfo.cnio.es/). The m^6A-seq sequencing data have been deposited in SRA PRJNA661159 (the data are being processed; submission ID: SUB8069560, to be released when the paper is published). The processed data and basic association analyses will be made available in supplementary data or from the corresponding author on reasonable request.

Statistical analysis

Univariate and multivariate Cox regression models, least absolute shrinkage and selection operator (LASSO) regression, and receiver operating characteristic (ROC) curve analysis were performed using RStudio (version 3.5.2). Kaplan–Meier survival curves were drawn using GraphPad Prism 7.04, and significant differences were compared by the log-rank (Mantel-Cox) test between two groups. Quantitative data are presented as the mean ± SEM. Student's t-test was used for two-group comparisons, and one-way analysis of variance (ANOVA) was used for three-group comparisons. $P \leq 0.05$ was considered statistically significant. (*$P \leq 0.05$, **$P \leq 0.01$, ***$P \leq 0.001$, ****$P \leq 0.0001$). All data processing with R packages was performed using R Studio (version 3.6.3).

Abbreviations

M^6A: N^6-Methyladenosine; GBM: Glioblastoma; MTC: m^6A methyltransferase complex; LASSO: Least absolute shrinkage and selection operator; ROC: Receiver operating characteristic; AUC: Area under curve; METTL3/14: Methyltransferase-like 3 and 14; WTAP: Wilms tumor 1-associated protein; WGCNA: Weighted Gene Co-Expression Network Analysis; IDH: Isocitrate dehydrogenase; G-CIMP: CpG island methylator phenotype; MGMT: O6-methylguanine-DNA methyltransferase; TCGA: The Cancer Genome Atlas; CGGA: Chinese Glioma Genome Atlas; AURKB：Aurora kinase B; CDC25C: Cell division cycle 25C; CENPE: Centromere protein E; ECT2: Epithelial cell transforming 2; FOXM1: Forkhead box M1; KIFC1: Kinesin family member C1; MCM10: Minichromosome maintenance complex component 10; TRIP13: Thyroid hormone receptor interactor 13;

Declarations

Acknowledgements

We thank the surgeons and patients who participated in these studies; the Novogene Co. Ltd and Tianjin Novogene Bioinformatics Technology Co., Ltd for m6A technical development and support.

Authors' contributions

GL and HX supervised the project. RRZ designed the research and executed all the results; BYL and ZH provided the statistical analysis of R language code; SJZ, QDG, PZ, and WQ were responsible for clinical sample collection and delivery. YHQ, XLZ, ZWP and XG help to revise the manuscript. All authors read and approved the final manuscript.

Funding

This work was supported by grants from the National Natural Science Foundation of China (Nos. 81874083; 82072776; 82072775; 81702468; 81802966; 81902540), Natural Science Foundation of Shandong Province of China (Nos. ZR2019BH057，ZR2020QH174), Key clinical Research project of Clinical Research Center of Shandong University (2020SDUCRCA011) and Taishan Scholars of Shandong Province of China (No. ts201511093).

Availability of data

All data used in this work can be acquired from TCGA database (http://cancergenome.nih.gov/), UCSC database (https://xena.ucsc.edu/public), Gliovis database (http://gliovis.bioinfo.cnio.es/), CGGA database (http://www.cgga.org.cn/). The m^6A-seq sequencing data have been deposited in SRA PRJNA661159. And the processed data and basic association analyses will be made available in supplementary data or from the corresponding author on reasonable request.

Ethics approval and consent to participate

All participants provided written informed consent, and the research was approved by the Ethical Committee on Scientific Research of Shandong University Qilu Hospital (approval number: KYLL-2018-324).

Consent for publication

Not applicable.

Competing interests

The authors declare they have no competing interests.

Author details

[1]Department of Neurosurgery, Qilu Hospital, Cheeloo College of Medicine and Institute of Brain and Brain-Inspired Science, Shandong University, Jinan 250012, Shandong, China;

[2]Shandong Key Laboratory of Brain Function Remodeling, Jinan 250012, Shandong, China

References

1. Dominissini D, Moshitch-Moshkovitz S, Schwartz S, Salmon-Divon M, Ungar L, Osenberg S, Cesarkas K, Jacob-Hirsch J, Amariglio N, Kupiec M, Sorek R, G Rechavi: Topology of the human and mouse m6A RNA methylomes revealed by m6A-sEq. *Nature* 2012, 485(7397):201–206.
2. Meyer KD, Saletore Y, Zumbo P, Elemento O, Mason CE, Jaffrey SR. Comprehensive analysis of mRNA methylation reveals enrichment in 3' UTRs and near stop codons. Cell. 2012;149(7):1635–46.
3. Zhao X, Yang Y, Sun BF, Shi Y, Yang X, Xiao W, Hao YJ, Ping XL, Chen YS, Wang WJ, Jin KX, Wang X, Huang CM, Fu Y, Ge XM, Song SH, Jeong HS, Yanagisawa H, Niu Y, Jia GF, Wu W, Tong WM, Okamoto A, He C, Danielsen JMR, Wang XJ, Yang YG. FTO-dependent demethylation of N6-methyladenosine regulates mRNA splicing and is required for adipogenesis. Cell research. 2014;24(12):1403–19.
4. Meyer KD, Patil DP, Zhou J, Zinoviev A, Skabkin MA, Elemento O, Pestova TV, Qian SB. SR Jaffrey: 5' UTR m(6)A Promotes Cap-Independent Translation. Cell. 2015;163(4):999–1010.
5. Wang X, Zhao BS, Roundtree IA, Lu Z, Han D, Ma H, Weng X, Chen K, Shi H, He C. N(6)-methyladenosine Modulates Messenger RNA Translation Efficiency. Cell. 2015;161(6):1388–99.
6. Wang X, Lu Z, Gomez A, Hon GC, Yue Y, Han D, Fu Y, Parisien M, Dai Q, Jia G, Ren B, Pan T, He C. N6-methyladenosine-dependent regulation of messenger RNA stability. Nature. 2014;505(7481):117–20.
7. Shi H, Wang X, Lu Z, Zhao BS, Ma H, Hsu PJ, Liu C, He C. YTHDF3 facilitates translation and decay of N-methyladenosine-modified RNA. Cell research. 2017;27(3):315–28.
8. Yang Y, Hsu PJ, Chen YS, Yang YG. Dynamic transcriptomic mA decoration: writers, erasers, readers and functions in RNA metabolism. Cell research. 2018;28(6):616–24.

9. Deng X, Su R, Weng H, Huang H, Li Z, Chen J. RNA N-methyladenosine modification in cancers: current status and perspectives. Cell research. 2018;28(5):507–17.
10. Jian W, Peled-Zehavi H, Galili G: The m A reader ECT2 post-transcriptionally regulates proteasome activity in Arabidopsis. *The New phytologist* 2020.
11. Li F, Zhang C, Zhang G. m6A RNA Methylation Controls Proliferation of Human Glioma Cells by Influencing Cell Apoptosis. Cytogenet Genome Res. 2019;159(3):119–25.
12. Cui Q, Shi H, Ye P, Li L, Qu Q, Sun G, Sun G, Lu Z, Huang Y, Yang CG, Riggs AD, He C, Shi Y. mA RNA Methylation Regulates the Self-Renewal and Tumorigenesis of Glioblastoma Stem Cells. Cell reports. 2017;18(11):2622–34.
13. Zhang S, Zhao BS, Zhou A, Lin K, Zheng S, Lu Z, Chen Y, Sulman EP, Xie K, Bögler O, Majumder S, He C, Huang S. mA Demethylase ALKBH5 Maintains Tumorigenicity of Glioblastoma Stem-like Cells by Sustaining FOXM1 Expression and Cell Proliferation Program. Cancer cell. 2017;31(4):591–606.e596.
14. Visvanathan A, Patil V, Arora A, Hegde AS, Arivazhagan A, Santosh V, Somasundaram K. Essential role of METTL3-mediated mA modification in glioma stem-like cells maintenance and radioresistance. Oncogene. 2018;37(4):522–33.
15. Li F, Yi Y, Miao Y, Long W, Long T, Chen S, Cheng W, Zou C, Zheng Y, Wu X, Ding J, Zhu K, Chen D, Xu Q, Wang J, Liu Q, Zhi F, Ren J, Cao Q, Zhao W. N-Methyladenosine Modulates Nonsense-Mediated mRNA Decay in Human Glioblastoma. Cancer research. 2019;79(22):5785–98.
16. Fu Y, Dominissini D, Rechavi G, He C. Gene expression regulation mediated through reversible m^6A RNA methylation. Nature reviews Genetics. 2014;15(5):293–306.
17. Chen T, Hao YJ, Zhang Y, Li MM, Wang M, Han W, Wu Y, Lv Y, Hao J, Wang L, Li A, Yang Y, Jin KX, Zhao X, Li Y, Ping XL, Lai WY, Wu LG, Jiang G, Wang HL, Sang L, Wang XJ, Yang YG, Q Zhou: m(6)A RNA methylation is regulated by microRNAs and promotes reprogramming to pluripotency. *Cell stem cell* 2015, 16(3):289–301.
18. Zhou Y, Zhou B, Pache L, Chang M, Khodabakhshi AH, Tanaseichuk O, Benner C, Chanda SK. Metascape provides a biologist-oriented resource for the analysis of systems-level datasets. Nature communications. 2019;10(1):1523.
19. Langfelder P, Horvath S. WGCNA: an R package for weighted correlation network analysis. BMC Bioinform. 2008;9:559.
20. Tsuno T, Natsume A, Katsumata S, Mizuno M, Fujita M, Osawa H, Nakahara N, Wakabayashi T, Satoh Y, Inagaki M, Yoshida J: Inhibition of Aurora-B function increases formation of multinucleated cells in p53 gene deficient cells and enhances anti-tumor effect of temozolomide in human glioma cells. *Journal of neuro-oncology* 2007, 83(3):249–258.
21. Aasland D, Götzinger L, Hauck L, Berte N, Meyer J, Effenberger M, Schneider S, Reuber EE, Roos WP, Tomicic MT, Kaina B, Christmann M. Temozolomide Induces Senescence and Repression of DNA Repair Pathways in Glioblastoma Cells via Activation of ATR-CHK1, p21, and NF-κB. Cancer research. 2019;79(1):99–113.

22. Navis AC, van den Eijnden M, Schepens JT, Hooft van R, Huijsduijnen P, Wesseling WJ Hendriks: Protein tyrosine phosphatases in glioma biology. *Acta neuropathologica* 2010, 119(2):157–175.
23. Rath O, Kozielski F. Kinesins and cancer. Nature reviews Cancer. 2012;12(8):527–39.
24. Li F, Yi Y, Miao Y, Long W, Long T, Chen S, Cheng W, Zou C, Zheng Y, Wu X, Ding J, Zhu K, Chen D, Xu Q, Wang J, Liu Q, Zhi F, Ren J, Cao Q, Zhao W. N-Methyladenosine Modulates Nonsense-Mediated mRNA Decay in Human Glioblastoma. Cancer research. 2019;79(22):5785–98.
25. Visvanathan A, Patil V, Arora A, Hegde AS, Arivazhagan A, Santosh V, Somasundaram K. Essential role of METTL3-mediated mA modification in glioma stem-like cells maintenance and radioresistance. Oncogene. 2018;37(4):522–33.
26. Zhang C, Han X, Xu X, Zhou Z, Chen X, Tang Y, Cheng J, Moazzam NF, Liu F, Xu J, Peng W, Du F, Zhang B, Song Z, Zeng J. A Gong: FoxM1 drives ADAM17/EGFR activation loop to promote mesenchymal transition in glioblastoma. Cell death disease. 2018;9(5):469.
27. Yoon KJ, Ringeling FR, Vissers C, Jacob F, Pokrass M, Jimenez-Cyrus D, Su Y, Kim NS, Zhu Y, Zheng L, Kim S, Wang X, Doré LC, Jin P, Regot S, Zhuang X, Canzar S, He C, Ming GL, Song H. Temporal Control of Mammalian Cortical Neurogenesis by mA Methylation. Cell. 2017;171(4):877–89.e817.
28. Venuto S, Monteonofrio L, Cozzolino F, Monti M, Appolloni I, Mazza T, Canetti D, Giambra V, Panelli P, Fusco C, Squeo GM, Croce AI, Pucci P, Malatesta P, Soddu S, Merla G, Micale L. TRIM8 interacts with KIF11 and KIFC1 and controls bipolar spindle formation and chromosomal stability. Cancer letters. 2020;473:98–106.
29. Thu YM, Bielinsky AK. Enigmatic roles of Mcm10 in DNA replication. Trends Biochem Sci. 2013;38(4):184–94.
30. Bell SP, Dutta A. DNA replication in eukaryotic cells. Annual review of biochemistry. 2002;71:333–74.
31. Clairmont CS, Sarangi P, Ponnienselvan K, Galli LD, Csete I, Moreau L, Adelmant G, Chowdhury D, Marto JA. AD D'Andrea: TRIP13 regulates DNA repair pathway choice through REV7 conformational change. Nat Cell Biol. 2020;22(1):87–96.
32. Zhang G, Zhu Q, Fu G, Hou J, Hu X, Cao J, Peng W, Wang X, Chen F, Cui H. TRIP13 promotes the cell proliferation, migration and invasion of glioblastoma through the FBXW7/c-MYC axis. British journal of cancer. 2019;121(12):1069–78.
33. Arribas-Hernández L, Bressendorff S, Hansen MH, Poulsen C, Erdmann S, Brodersen P. An mA-YTH Module Controls Developmental Timing and Morphogenesis in Arabidopsis. Plant Cell. 2018;30(5):952–67.
34. Shan L, Zhao M, Lu Y, Ning H, Yang S, Song Y, Chai W, Shi X. CENPE promotes lung adenocarcinoma proliferation and is directly regulated by FOXM1. Int J Oncol. 2019;55(1):257–66.
35. Zhou K, Mai H, Zheng S, Cai W, Yang X, Chen Z, Zhan B. OTUB1-mediated deubiquitination of FOXM1 up-regulates ECT-2 to promote tumor progression in renal cell carcinoma. Cell bioscience. 2020;10:50.
36. Yang Y, Hsu PJ, Chen YS, Yang YG. Dynamic transcriptomic mA decoration: writers, erasers, readers and functions in RNA metabolism. Cell research. 2018;28(6):616–24.

Figures

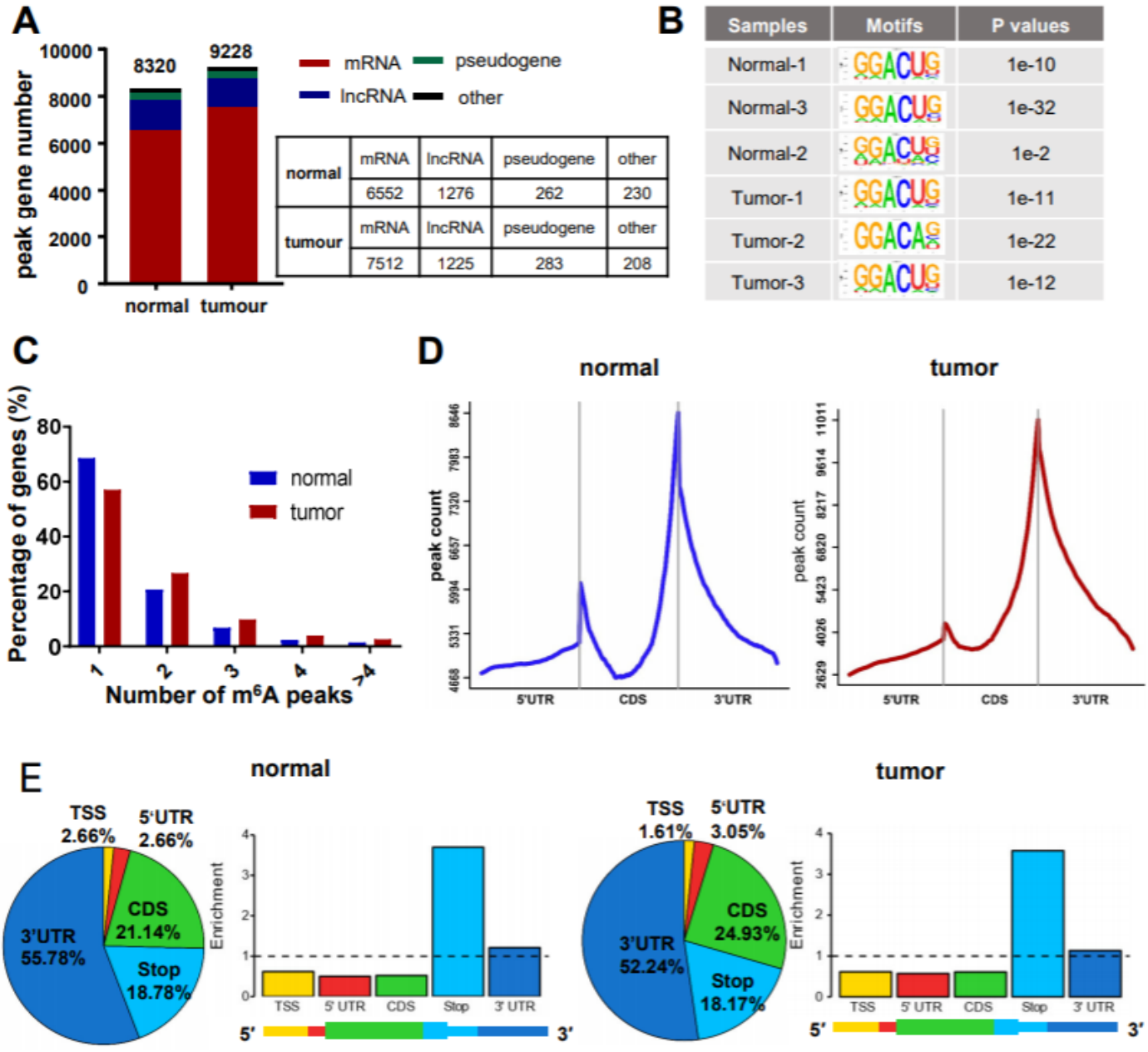

Figure 1

Overview of N6-methyladenosine methylation within mRNAs in the GBM and normal brain tissues. (A). The number of genes and gene types identified in normal brain and GBM tissue samples identified by m6A-seq; (B) Predominant consensus motif “GGAC” was detected in both the normal and GBM tissues in m6A-seq; (C) The number of m6A-modified peaks per gene; (D) Density distribution of m6A peaks across mRNA transcripts in normal brain tissues (left) and GBM tissues (right); (E) Left: pie chart presenting the proportion of m6A peaks in each of five non-overlapping gene segments; right: histogram presenting the

relative enrichment of m6A peaks across gene segments; bottom of the histogram: schematic of the five segments.

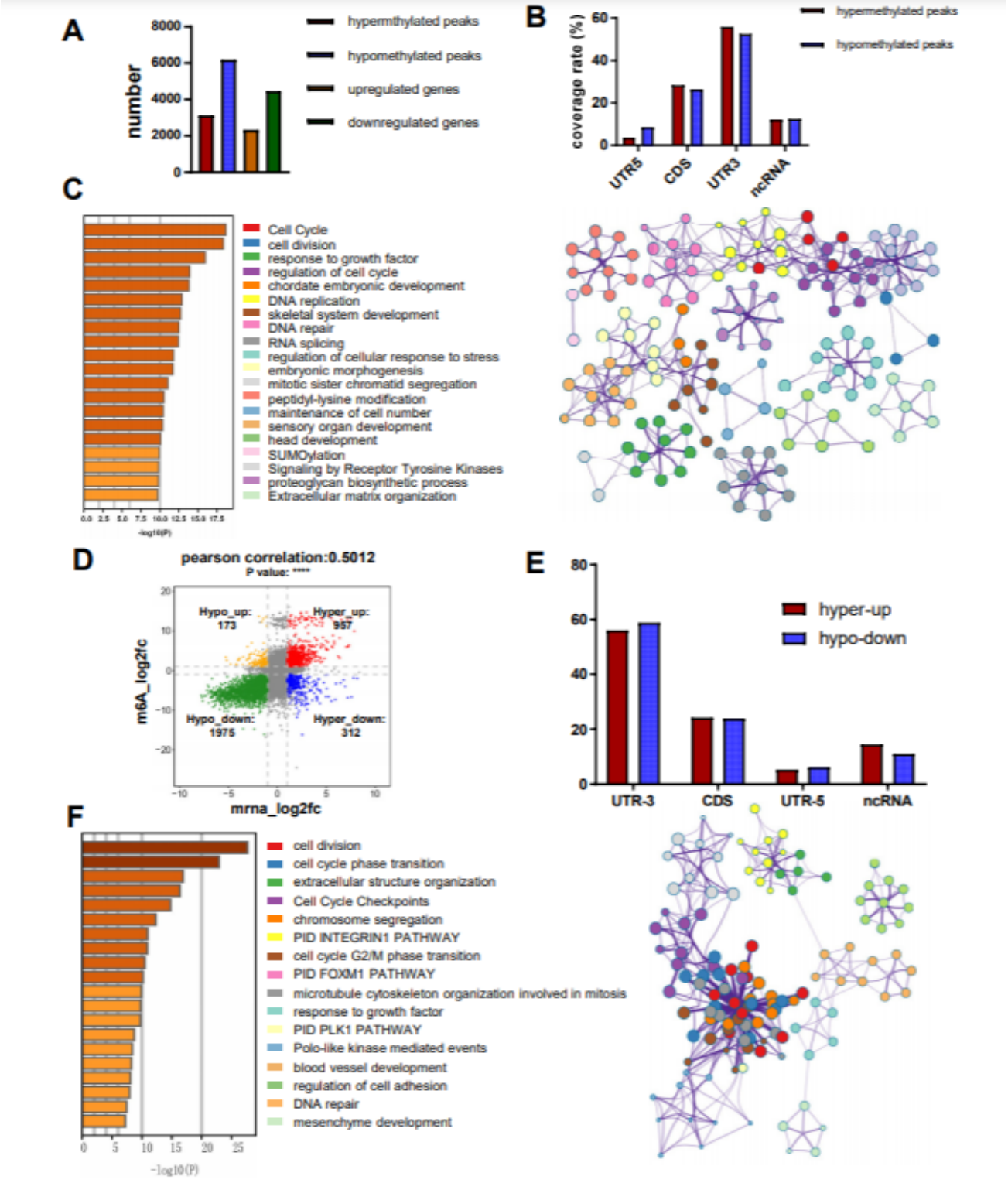

Figure 2

Global m6A modification and expression changes in GBM tissues compared with normal brain tissues. (A) Count of differentially m6A-modified peaks and corresponding genes in the normal and GBM tumour brain; (B) The coverage rate of m6A peak distribution of hyper- and hypo-methylated genes; (C) Bar graph

of enriched terms across upregulated genes, coloured by p-values, and corresponding network of enriched terms; (D) Dot plot of Log2FC (mRNA expression) against Log2FC (differential m6A methylation) showing a positive correlation between overall m6A methylation and mRNA expression level (Pearson r=0.5012; p□0.0001) and distribution of genes with a significant change in both m6A (FC≥1.2, p≤0.05) and mRNA levels in GBM samples compared with normal brain tissues (FC≥2, FDR≤0.05); (E) The coverage rate of m6A peak distribution of hyper-up and hypo-down genes; (F) Bar graph of enriched terms across hyper-up genes, coloured by p-values, and corresponding network of enriched terms.

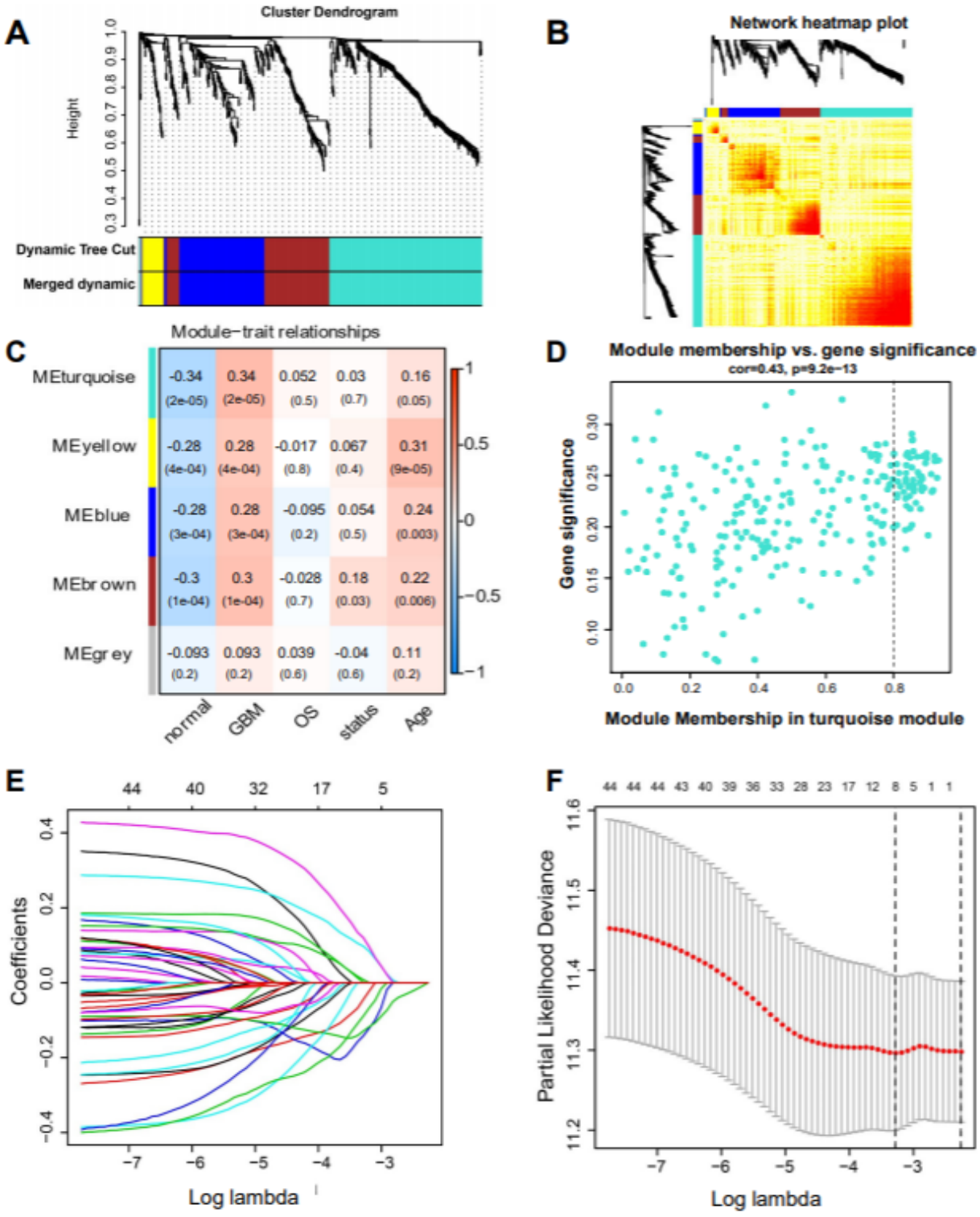

Figure 3

Weighted co-expression network construction and key module identification. (A) Cluster dendrogram indicating hyper-up gene modules; (B) Heatmap describing the TOM among hyper-up genes in WGCNA; (C) Heatmap of the correlation between module eigengenes with the disease progression and other clinico-pathological features of GBM; (D) Scatter plot of module eigengenes in turquoise module; (E) Log (Lambda) value of the 44 genes in the LASSO model; (F) The most appropriate log (Lambda) value in the LASSO model.

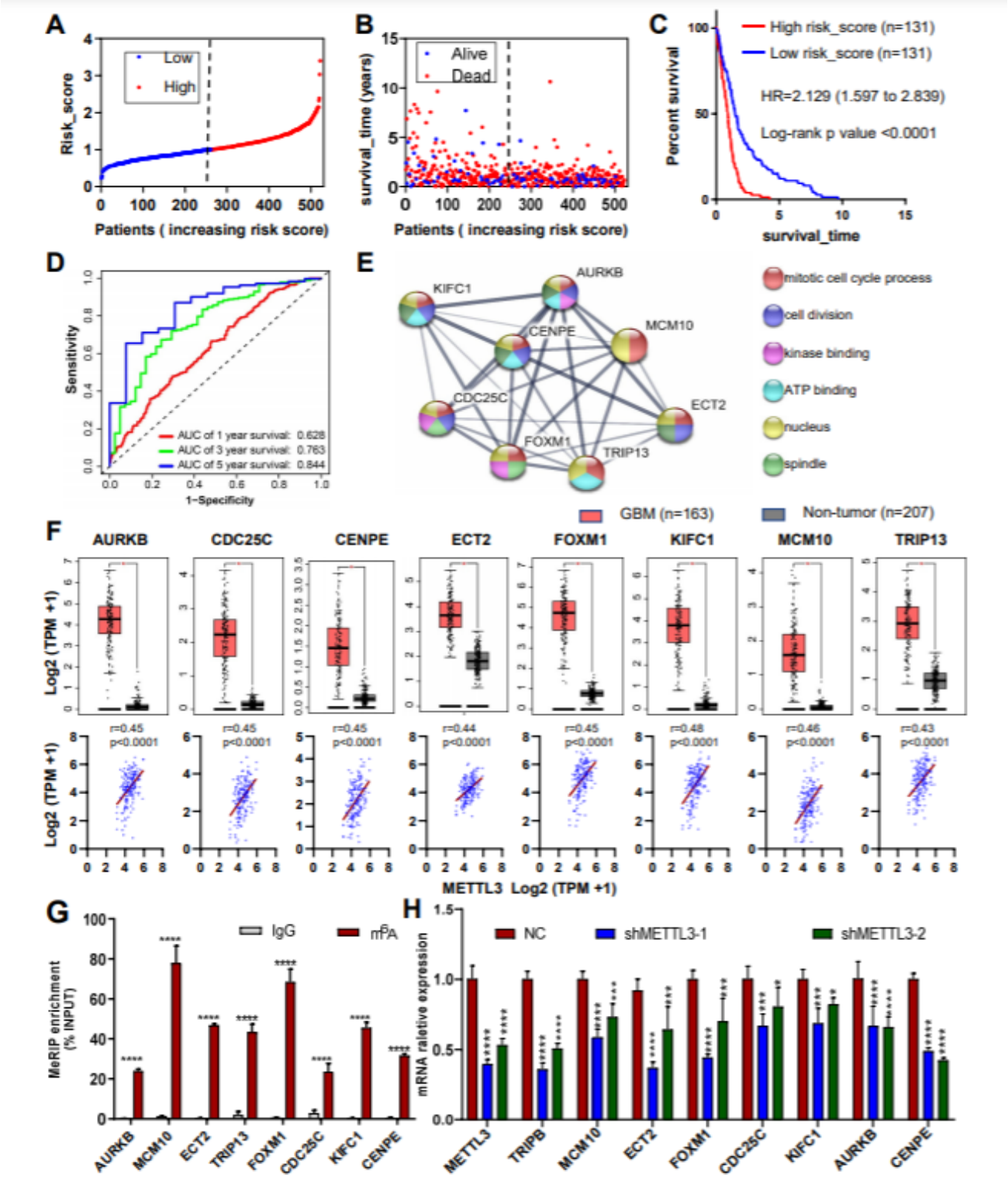

Figure 4

The efficiencies of the 8-gene m6A-related epigenetic signature in the TCGA GBM datasets. (A) the risk scores distribution and (B) patients' survival status of the 8 m6A-related gene expression profiles in the TCGA GBM array dataset; (C) The Kaplan-Meier survival curves showing the prognostic value of the risk signature in the TCGA GBM array dataset in quartile group cut-offs; (D) ROC curves evaluating the efficiency of the 8 m6A-related risk signature for predicting 1-, 3- and 5-year survival in the TCGA GBM array dataset; (E) Protein–protein interaction network and GO analysis of the 8 m6A-related genes via the string database; (F) The expression of the 8 m6A-related genes in GBM samples (n=163) compared with GETx normal brain tissues (n=207) via the GEPIA database; (G) The correlation of METTL3 with the 8 m6A-related genes in TCGA GBM samples; (H) MeRIP-qPCR assays showed that the 8 genes could be modified by m6A. Data represent mean ± SEM from three independent experiments. $P \leq 0.05$ was considered statistically significant (*$P \leq 0.05$; **$P \leq 0.01$; ***$P \leq 0.001$, ****$P \leq 0.0001$); (I) QPCR assays showed that all the 8 genes could be positively regulated by m6A methyltransferase METTL3. Data represent mean ± SEM from three independent experiments. $P \leq 0.05$ was considered statistically significant (*$P \leq 0.05$; **$P \leq 0.01$; ***$P \leq 0.001$, ****$P \leq 0.0001$).

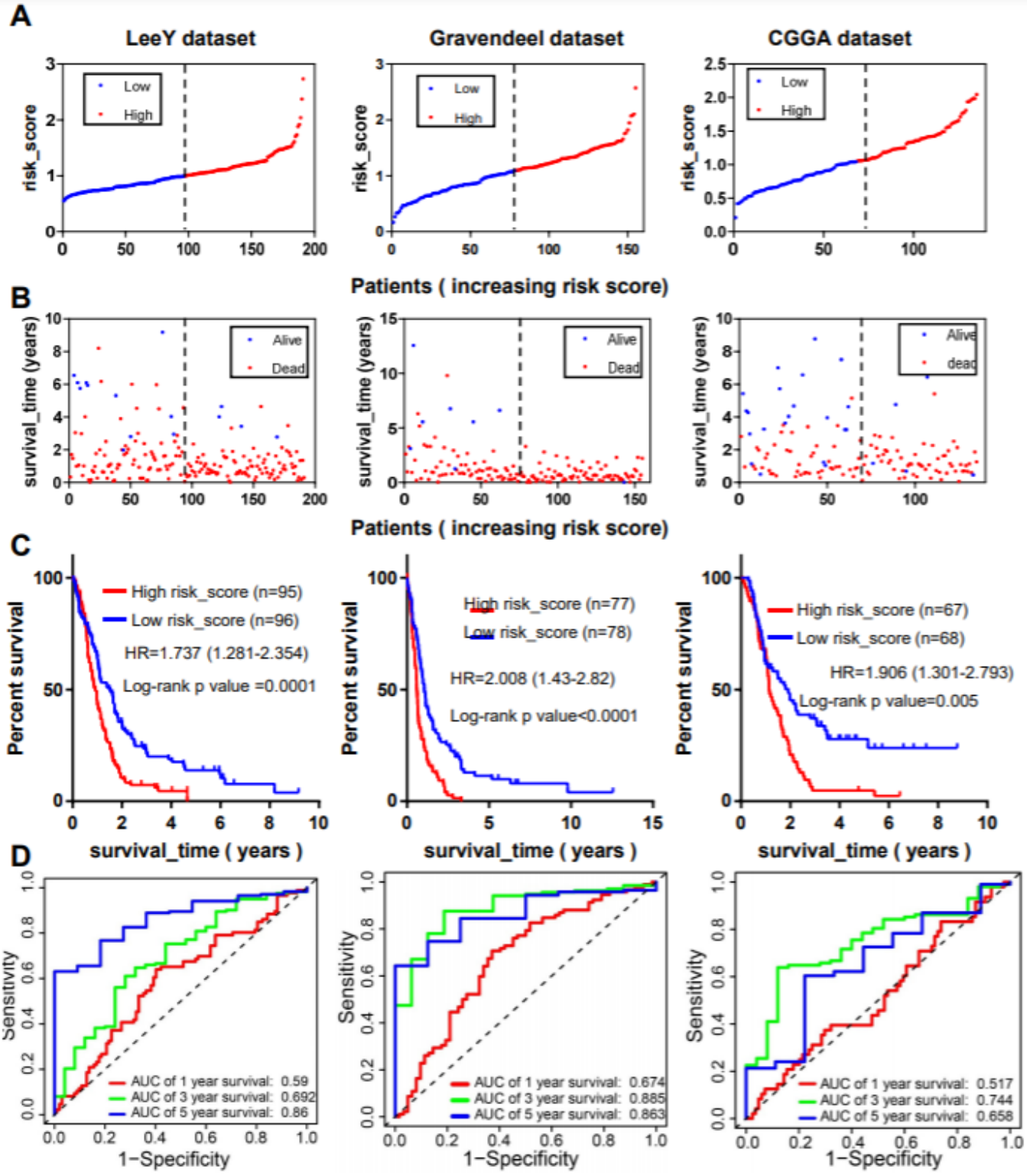

Figure 5

Validating the efficiencies of the m6A-related 8-gene epigenetic signature in the three datasets. (A) The risk score distribution of the m6A-related 8-gene signature; (B) The patients' survival status of the m6A-related 8-gene signature in the LeeY dataset (left), Gravendeel dataset (middle) and right dataset (right); (C) The Kaplan-Meier survival curves showed the prognostic value of the risk signature in LeeY dataset (left), Gravendeel dataset (middle) and right dataset (right) in the median group cut-off; (D) ROC curves

evaluating the efficiency of the 8 m6A-related risk gene signature for predicting 1-, 3- and 5-year survival in the LeeY dataset (left), Gravendeel dataset (middle) and right dataset (right);

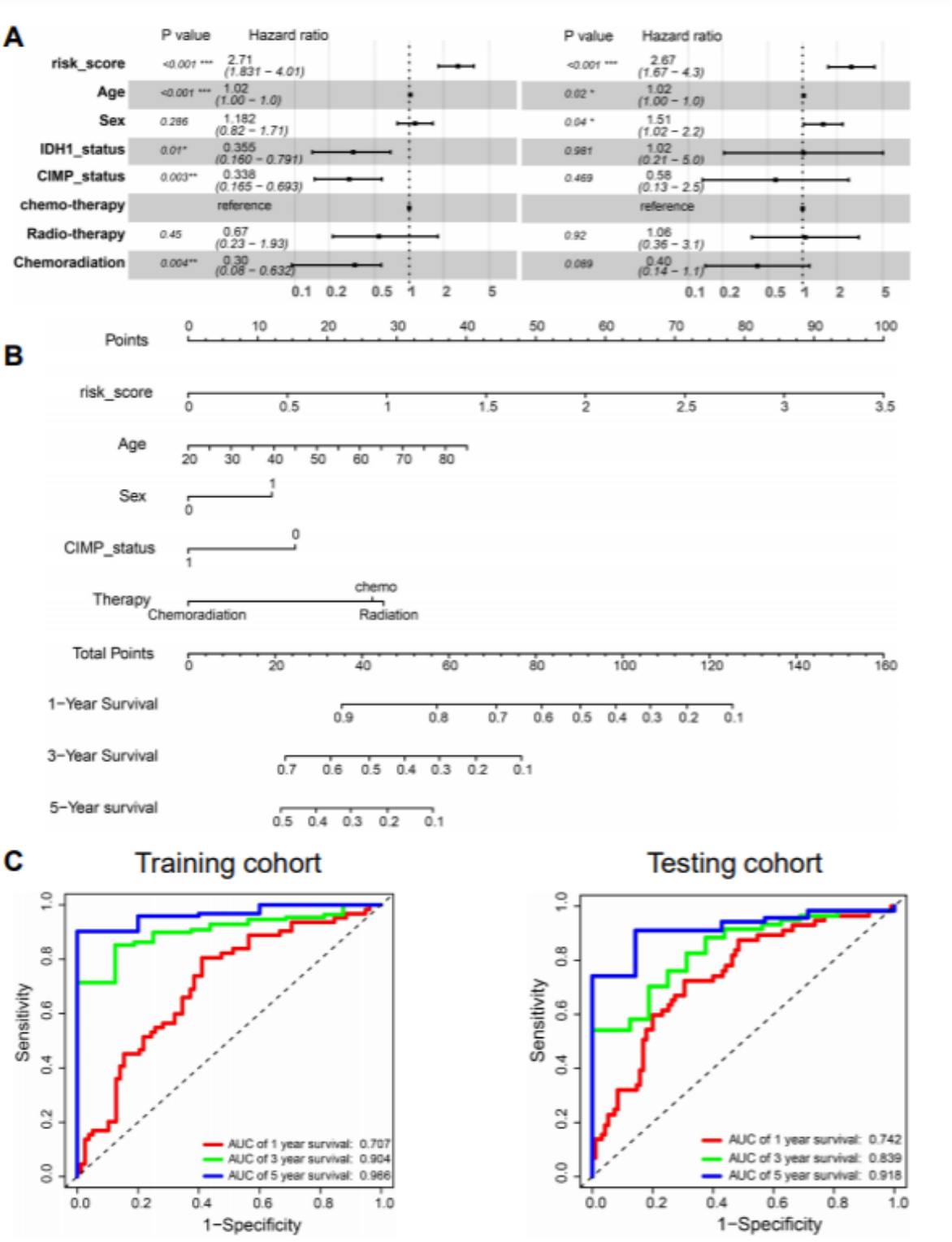

Figure 6

Construction of a nomogram for predicting 1-, 3- and 5-year survival rates of GBM. (A) Univariate and multivariate Cox regression analyses evaluated the contribution of each factor to GBM survival in the training cohort; Sex: male vs female; IDH-status: mutant vs wildtype; CIMP-status: G-CIMP vs NON G-

CIMP; (B) A nomogram for predicting 1-, 3- and 5-year survival rates of GBM patients was constructed; (C) ROC curves evaluating the high accuracy of the nomogram for predicting 1-, 3- and 5-year survival in the training cohort (left) and validation cohort (right).

Supplementary Files

This is a list of supplementary files associated with this preprint. Click to download.

- Additionalfile1.Supplementaryresults.docx
- Additionalfile2.Supplementarymethods.docx
- Additionalfile3.TableS1Tumourallpeakgenes.xlsx
- Additionalfile4.TableS2Normalallpeakgenes.xlsx
- Additionalfile5.TableS3DiffmRNAsGBMvsnormal.xlsx
- Additionalfile6.TableS4DiffmRNAsHighvsLowrisk.xlsx
- Additionalfile7.TableS5Enrichedhallmark.xlsx
- Additionalfile8.TableS6EnrichedKEGGpathway.xlsx